J. Fluid Mech. (2015), *vol.* 782, *pp.* 25–36.
doi:10.1017/jfm.2015.538

On the kurtosis of deep-water gravity waves

Francesco Fedele[1,2,†]

[1]School of Civil and Environmental Engineering, Georgia Institute of Technology, Atlanta, GA 30322, USA

[2]School of Electrical and Computer Engineering, Georgia Institute of Technology, Atlanta, GA 30322, USA

(Received 28 December 2014; revised 5 June 2015; accepted 8 September 2015)

In this paper, we revisit Janssen's (*J. Phys. Oceanogr.*, vol. 33 (4), 2003, pp. 863–884) formulation for the dynamic excess kurtosis of weakly nonlinear gravity waves in deep water. For narrowband directional spectra, the formulation is given by a sixfold integral that depends upon the Benjamin–Feir index and the parameter $R = \sigma_\theta^2/2\nu^2$, a measure of short-crestedness for the dominant waves, with ν and σ_θ denoting spectral bandwidth and angular spreading. Our refinement leads to a new analytical solution for the dynamic kurtosis of narrowband directional waves described with a Gaussian-type spectrum. For multidirectional or short-crested seas initially homogeneous and Gaussian, in a focusing (defocusing) regime dynamic kurtosis grows initially, attaining a positive maximum (negative minimum) at the intrinsic time scale $\tau_c = \nu^2\omega_0 t_c = 1/\sqrt{3R}$, or $t_c/T_0 \approx 0.13/\nu\sigma_\theta$, where $\omega_0 = 2\pi/T_0$ denotes the dominant angular frequency. Eventually the dynamic excess kurtosis tends monotonically to zero as the wave field reaches a quasi-equilibrium state characterized by nonlinearities mainly due to bound harmonics. Quasi-resonant interactions are dominant only in unidirectional or long-crested seas where the longer-time dynamic kurtosis can be larger than that induced by bound harmonics, especially as the Benjamin–Feir index increases. Finally, we discuss the implication of these results for the prediction of rogue waves.

Key words: surface gravity waves, wave-turbulence interactions, waves/free-surface flows

1. Introduction

Third-order quasi-resonant interactions and associated modulational instabilities cause the statistics of weakly nonlinear gravity waves to significantly differ from the Gaussian structure of linear seas (Janssen 2003; Fedele 2008; Onorato *et al.* 2009; Shemer & Sergeeva 2009; Toffoli *et al.* 2010; Xiao *et al.* 2013). One integral statistic used as a measure of the relative importance of such nonlinearities is the excess kurtosis defined by Janssen (2003) as

$$C_4 = \frac{\langle \eta^4 \rangle}{3\sigma^4} - 1, \tag{1.1}$$

† Email address for correspondence: fedele@gatech.edu

where η is the surface displacement with respect to the mean sea level, $\sigma^2 = \langle\eta^2\rangle$ is the wave variance and angle brackets denote a statistical average. In general,

$$C_4 = C_4^d + C_4^b, \tag{1.2}$$

which comprises a dynamic component C_4^d due to nonlinear wave–wave interactions (Janssen 2003) and a bound contribution C_4^b induced by the characteristic crest–trough asymmetry of ocean waves (see e.g. Tayfun 1980; Tayfun & Lo 1990; Tayfun & Fedele 2007; Fedele & Tayfun 2009). If third-order Stokes contributions are taken into account (Janssen 2009, 2014*b*; Janssen & Bidlot 2009) then

$$C_4^b = 6\mu^2. \tag{1.3}$$

For unidirectional (long-crested) seas initially homogeneous and Gaussian on deep water, Mori & Janssen (2006) have shown that the large-time behaviour of the dynamic excess kurtosis is to monotonically increase towards the asymptotic value

$$C_{4,NLS}^d = \mathrm{BFI}^2 \frac{\pi}{3\sqrt{3}}, \tag{1.4}$$

where

$$\mathrm{BFI} = \frac{\mu\sqrt{2}}{\nu} \tag{1.5}$$

is the Benjamin–Feir index, $\mu = k_0\sigma$ represents an integral measure of wave steepness, ν is the spectral bandwidth and k_0 is the dominant wavenumber. The preceding approximation is valid for the dynamics of unidirectional narrowband waves described by one-dimensional (1-D) nonlinear Schrödinger (NLS) and Dysthe (1979) equations (see, for example, Shemer & Sergeeva 2009; Shemer, Sergeeva & Liberzon 2010*a*; Shemer, Sergeeva & Slunyaev 2010*b*).

Clearly, the preceding results are valid for unidirectional waves where energy is ‘trapped’ as in a long wave-guide. If dissipation is negligible and the wave steepness is small, quasi-resonant interactions are effective in reshaping the wave spectrum, inducing nonlinear focusing and large waves in the form of breathers via modulation instability before breaking occurs (Onorato *et al.* 2009; Shemer & Sergeeva 2009; Shemer *et al.* 2010*a*; Chabchoub, Hoffmann & Akhmediev 2011; Chabchoub *et al.* 2012; Shemer & Alperovich 2013; Shemer & Liberzon 2014). However, such 1-D conditions never occur in nature as they are unrealistic models of oceanic wind seas. The latter are typically multidirectional (short-crested) and energy can spread directionally. As a result, nonlinear focusing due to modulational effects is reduced (Onorato *et al.* 2009; Waseda, Kinoshita & Tamura 2009; Toffoli *et al.* 2010).

In regard to the kurtosis in short-crested seas initially homogeneous and Gaussian, the focus of recent numerical studies has been on the asymptotic behaviour with time (see, for example, Annenkov & Shrira 2013, 2014; Janssen & Bidlot 2009). Theoretical studies on the transient short-lived features of kurtosis and their relevance to the prediction of rogue waves are desirable. These provide the principal motivation for revisiting Janssen’s (2003) formulation for the dynamic excess kurtosis of weakly nonlinear deep-water gravity waves.

The remainder of the paper is organized as follows. We first review Janssen’s (2003) dynamic kurtosis model. Then, we present a new analytical solution of a sixfold integral that yields the growth rate of the dynamic excess kurtosis for narrowband Gaussian-shaped spectra. This is followed by a detailed study of its short-time evolution and long-time asymptotic behaviour and comparisons to numerical simulations and experiments. In concluding, we discuss the implications of these results for rogue wave prediction.

2. Dynamic excess kurtosis

Drawing on Janssen (2003) the dynamic excess kurtosis of weakly nonlinear sea states, initially homogeneous and Gaussian, is given by

$$C_4^d = \frac{4g}{\sigma^2}\mathrm{Re}\int T_{12}^{34}\delta_{12}^{34}\sqrt{\frac{\omega_4}{\omega_1\omega_2\omega_3}}G(t)E_1E_2E_3\,\mathrm{d}\omega_{1,2,3}\,\mathrm{d}\theta_{1,2,3}, \tag{2.1}$$

where the resonant function

$$G(t) = \frac{1-\exp(-\mathrm{i}\omega_{12}^{34}t)}{\omega_{12}^{34}}, \tag{2.2}$$

T_{12}^{34} is the Zakharov kernel (Zakharov 1968, 1999; Krasitskii 1994) as a function of the wavenumber vectors $\boldsymbol{k}_j = (k_j\cos(\theta_j), k_j\sin(\theta_j))$ and $\mathrm{Re}(x)$ denotes the real part of x. The sixfold integral in (2.1) is defined over the manifold

$$\boldsymbol{k}_1+\boldsymbol{k}_2-\boldsymbol{k}_3-\boldsymbol{k}_4=\boldsymbol{0} \tag{2.3}$$

or equivalently $\delta_{12}^{34}=\delta(\boldsymbol{k}_1+\boldsymbol{k}_2-\boldsymbol{k}_3-\boldsymbol{k}_4)$, where $\delta(\boldsymbol{k})$ is the Dirac delta. The frequency mismatch is given by $\omega_{12}^{34}=\omega_1+\omega_2-\omega_3-\omega_4$, $E(\omega,\theta)$ is the surface spectrum and σ^2 is the variance of surface elevations. The deep-water angular frequency $\omega(k)=\sqrt{gk}$, the wavenumber magnitude $k=|\boldsymbol{k}|$, and

$$\omega_4=\sqrt{gk_4}=\sqrt{g|\boldsymbol{k}_1+\boldsymbol{k}_2-\boldsymbol{k}_3|} \tag{2.4}$$

follows from (2.3), with g denoting gravity acceleration. Since homogeneous Gaussian initial conditions with random phases and amplitudes are imposed, it follows that

$$C_4^d(t=0)=0. \tag{2.5}$$

Equation (2.1) can be simplified by resorting to a narrowband approximation (Mori & Janssen 2006; Janssen & Bidlot 2009). So, we assume the spectrum E to peak at $\omega=\omega_0$ and $\theta=\theta_0$, where ω_0 and θ_0 denote the dominant angular frequency and wave direction, respectively, and the associated wavenumber $k_0=\omega_0^2/g$, wave period $T_0=2\pi/\omega_0$ and phase speed $c_0=\omega_0/k_0$. Next, define

$$\omega_j=\omega_0(1+\nu v_j), \qquad \theta_j=\theta_0+\sigma_\theta\phi_j, \tag{2.6a,b}$$

where ν and σ_θ denote spectral and angular widths respectively. Under the narrowband condition $\nu,\sigma_\theta\ll 1$, $T_{12}^{34}\sim k_0^3$ to leading order and the frequency mismatch, correct to $O(\nu^2,\sigma_\theta^2)$, is given by

$$\omega_{12}^{34}\sim\nu^2\omega_0\Delta, \tag{2.7}$$

with

$$\Delta=\{(v_1-v_3)(v_2-v_3)-R(\phi_1-\phi_3)(\phi_2-\phi_3)\}=\Delta_v-R\Delta_\phi, \tag{2.8}$$

where $\Delta_z=(z_1-z_3)(z_2-z_3)$ for a generic $z=(z_1,z_2,z_3)$ triplet, and the parameter

$$R=\frac{1}{2}\frac{\sigma_\theta^2}{\nu^2} \tag{2.9}$$

is a measure of short-crestedness of dominant waves (Janssen & Bidlot 2009). Expanding (2.1) around $\nu=0$ and $\sigma_\theta=0$, to leading order

$$C_4^d(\tau)=\mathrm{BFI}^2 J(\tau;R), \tag{2.10}$$

where

$$J(\tau;R)=2\,\mathrm{Re}\int \frac{1-\exp(\mathrm{i}\Delta\tau)}{\Delta}\widetilde{E}_1\widetilde{E}_2\widetilde{E}_3\,\mathrm{d}v_{1,2,3}\,\mathrm{d}\phi_{1,2,3}. \tag{2.11}$$

Here, $\tau=\nu^2\omega_0 t$ is a dimensionless time and $\widetilde{E}_j(v_j,\phi_j)=E_j/\sigma$.

For a Gaussian-shaped spectrum, the rate of change of C_4^d is explicitly given by

$$\frac{\mathrm{d}C_4^d}{\mathrm{d}\tau}=\mathrm{BFI}^2\frac{\mathrm{d}J}{\mathrm{d}\tau}, \tag{2.12}$$

and

$$\frac{\mathrm{d}J}{\mathrm{d}\tau}=\frac{\mathrm{d}J_0(\tau;1,R)}{\mathrm{d}\tau}=2\,\mathrm{Im}\left(\frac{1}{\sqrt{1-2\mathrm{i}\tau+3\tau^2}\sqrt{1+2\mathrm{i}R\tau+3R^2\tau^2}}\right), \tag{2.13}$$

where the function $J_0(\tau;P,Q)$ is defined in appendix A and $\mathrm{Im}(x)$ denotes the imaginary part of x. On this basis, the factor J in (2.10) follows by quadrature as

$$J(\tau;R)=2\,\mathrm{Im}\int_0^\tau \frac{1}{\sqrt{1-2\mathrm{i}\alpha+3\alpha^2}\sqrt{1+2\mathrm{i}R\alpha+3R^2\alpha^2}}\,\mathrm{d}\alpha. \tag{2.14}$$

For small times $\tau\ll 1$,

$$J(\tau;R)=\int_0^\tau ((1-R)\alpha+O(\alpha^2))\,\mathrm{d}\alpha=\frac{1}{2}(1-R)\tau^2 \tag{2.15}$$

and (2.10) yields

$$C_4^d\sim \mathrm{BFI}^2(1-R)\tau^2,\quad \tau\ll 1, \tag{2.16}$$

in agreement with Janssen & Bidlot (2009).

Note that the dynamic excess kurtosis in (2.10) is consistent with the evolution of weakly nonlinear narrowband wavetrains of the two-dimensional (2-D) NLS equation.

3. Intrinsic nonlinear time scale

The growth rate (2.12) of the dynamic C_4^d vanishes at the dimensionless time

$$\tau_c=\frac{1}{\sqrt{3R}}, \tag{3.1}$$

or in physical units

$$\frac{t_c}{T_0}=\frac{1}{2\pi}\sqrt{\frac{2}{3}}\frac{1}{\sigma_\theta\nu}\sim\frac{0.13}{\sigma_\theta\nu}, \tag{3.2}$$

where $T_0=2\pi/\omega_0$ is the dominant wave period. Further, the second derivative of C_4^d at τ_c is given by

$$\left.\frac{\mathrm{d}^2C_4^d}{\mathrm{d}\tau^2}\right|_{\tau=\tau_c}=-6\sqrt{3}R(1-R). \tag{3.3}$$

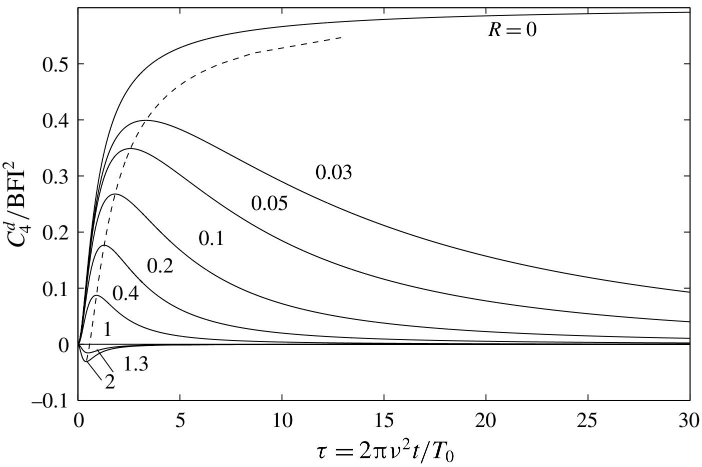

FIGURE 1. Dynamic excess kurtosis: solid lines, C_4^d/BFI^2 as a function of dimensionless time $\tau = \nu^2\omega_0 t = 2\pi\nu^2 t/T_0$ for different values of R; dashed line, locus of transient peaks (T_0 denotes the dominant wave period and ν is the spectral bandwidth).

Thus, C_4^d attains a positive maximum (negative minimum) at $\tau = \tau_c$ for $0 < R < 1$ ($R > 1$). It is straightforward to show that for multidirectional or short-crested seas ($R > 0$)

$$\lim_{\tau\to\infty} C_4^d = 0. \tag{3.4}$$

Indeed, it is sufficient to study the rate of change of C_4^d for large times $\tau \gg 1$. To do so, consider the change of variable $\tau = 1/r$ and expanding (2.12) around $r = 0$ yields

$$\frac{\mathrm{d}C_4^d}{\mathrm{d}\tau} \sim \frac{(-1+R)r^3}{9R^2} = \frac{(-1+R)}{9R^2\tau^3}. \tag{3.5}$$

Note that in (2.13) the real part of the term within parentheses, which has no physical meaning, decays as τ^{-2}. For $0 < R < 1$, C_4^d first attains a positive peak at $\tau = \tau_c$ and then decays monotonically to zero since $\mathrm{d}C_4^d/\mathrm{d}\tau < 0$ for large τ. This is clearly seen in figure 1, showing the evolution of C_4^d for different values of R. For $R > 1$, C_4^d initially decreases, reaching a negative peak at $\tau = \tau_c$, and then tends monotonically to zero, because $\mathrm{d}C_4^d/\mathrm{d}\tau > 0$ for large τ as shown in figure 1. At the critical value $R = 1$, the excess kurtosis is null at any time, as can easily be verified from (2.12).

In summary, depending on the value of R there will be nonlinear focusing ($C_4^d > 0$) or nonlinear defocusing ($C_4^d < 0$) in agreement with Janssen & Bidlot (2009). Note that for unidirectional or long-crested seas ($R = 0$) the rate of change $\mathrm{d}C_4^d/\mathrm{d}\tau > 0$ for any time τ. In this case, the dynamic excess kurtosis monotonically increases with time to the asymptotic value of (1.4) (Mori & Janssen 2006; Shemer & Sergeeva 2009; Fedele *et al.* 2010; Shemer *et al.* 2010*a*,*b*).

4. Dynamic excess kurtosis maximum

From (2.10) and (3.1), the peak value of C_4^d at $\tau = \tau_c$ is given by

$$C_4^d(R) = \mathrm{BFI}^2 J_p(R), \tag{4.1}$$

where

$$J_p(R) = J\left(\frac{1}{\sqrt{3R}}; R\right) = \mathrm{Im}\int_0^{1/\sqrt{3R}} \frac{2}{\sqrt{1-2\mathrm{i}\alpha+3\alpha^2}\sqrt{1+2\mathrm{i}R\alpha+3R^2\alpha^2}}\,\mathrm{d}\alpha. \quad (4.2)$$

The following relation holds:

$$J_p\left(\frac{1}{R}\right) = -RJ_p(R), \quad (4.3)$$

in agreement with Janssen & Bidlot (2009). This relation allows us to compute the minimum kurtosis for $R > 1$ from the maximum value for $R < 1$. Indeed,

$$C^d_{4,min}\left(\frac{1}{R}\right) = -RC^d_{4,max}(R), \quad 0 \leqslant R \leqslant 1, \quad (4.4)$$

where $C^d_{4,max} = \mathrm{BFI}^2 J_p(R)$. Clearly, this vanishes at $R = 1$ signalling the change from a nonlinear focusing to a defocusing regime where the dynamic excess kurtosis is negative.

Drawing on Janssen & Bidlot (2009), the limit

$$J_p(R) \sim -\frac{\pi}{3\sqrt{3R}}, \quad R \gg 1, \quad (4.5)$$

and that for small times in (2.16), suggest the least-squares fit for the maximum

$$\frac{C^d_{4,max}(R)}{\mathrm{BFI}^2} = J_{peak}(R) \approx \frac{b}{(2\pi)^2}\frac{1-R}{R+bR_0}, \quad 0 \leqslant R \leqslant 1, \quad (4.6)$$

where $R_0 = (3\sqrt{3})/\pi$ and $b = 2.48$. In figure 2(*a*), the preceding approximation is compared to the theoretical $C^d_{4,max}$ obtained from solving (4.1) by numerical integration. Evidently, the latter is slightly larger than the maximum excess kurtosis derived by Janssen & Bidlot (2009), who have also used (4.6) but with $b = 1$. Their maximum follows by first taking the limit of the resonant function $G(t)$ in (2.2) at $t = \infty$ and then solving the sixfold integral in (2.1). Clearly, for $R > 0$ the dynamic excess kurtosis should vanish at large times as discussed above. Janssen (personal communication, 2014*a*) confirmed that (4.1) holds and provided an alternative proof that C^d_4 tends to zero as $t \to \infty$ using complex analysis and numerical integration.

Further, from (3.1)

$$\frac{C^d_{4,max}(\tau_c)}{\mathrm{BFI}^2} \approx \frac{b}{(2\pi)^2}\frac{-1+3\tau_c^2}{1+3bR_0\tau_c^2}, \quad 0 \leqslant \tau_c \leqslant \frac{1}{\sqrt{3}}. \quad (4.7)$$

Clearly, the transient maximum kurtosis becomes larger for longer time scales τ_c, as illustrated in figure 2(*b*). Note that the dynamic excess kurtosis is negative for $\tau_c > 1/\sqrt{3}$ as the wave regime is of defocusing type ($R > 1$) and the minimum value $C^d_{4,min}$ can be computed from (4.4).

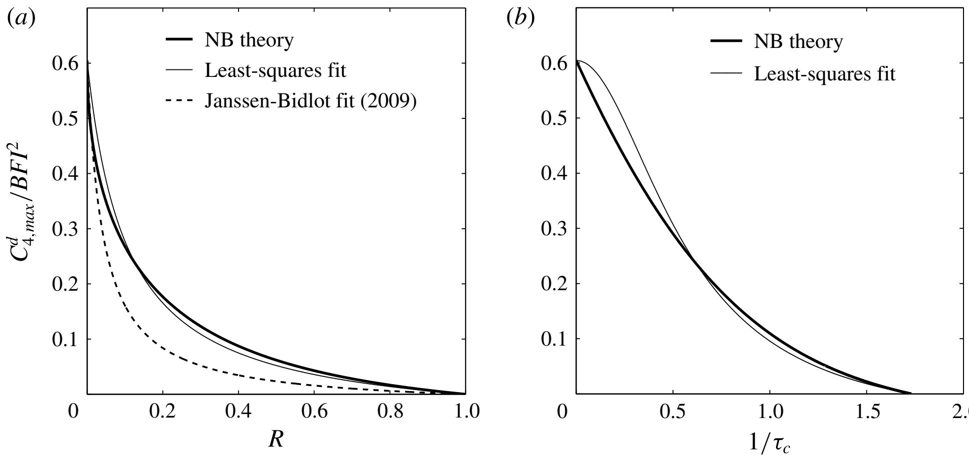

FIGURE 2. Maximum dynamic excess kurtosis $C^d_{4,max}$ as a function of (*a*) R and (*b*) $1/\tau_c$: bold line, present theoretical prediction; thin line, least-squares fit from (4.6) ($b = 2.48$); dashed line, Janssen & Bidlot (2009) fit ($b = 1$).

5. Comparisons to simulations and experiments

We now compare the theoretical narrowband (NB) predictions for the total kurtosis C_4 (see (1.2), (2.10) and (1.3)) to experimental results (Onorato *et al.* 2009) and the comprehensive numerical simulations of JONSWAP directional wave fields carried out by Toffoli *et al.* (2010) and Xiao *et al.* (2013). They considered the broadband modified nonlinear Schrödinger equations (BMNLS) (Dysthe 1979) and a high-order spectral (HOS) solver (Dommermuth & Yue 1987). In particular, we consider the comprehensive numerical results reported in figures 10(*a*,*b*) in Xiao *et al.* (2013) for the two cases of narrow and broad directional spreading, i.e. $\sigma_\theta = 0.04$ and 0.07 respectively. The simulated sea states have standard deviation $\sigma = 0.02$ m, dominant wave period $T_0 = 1$ s, significant wave height $H_s = 4\sigma = 0.08$ m, $\mathrm{BFI} = 0.78$, wave steepness $\mu = 0.08$ and spectral bandwidth $\nu = 0.15$ (see appendix B for the estimation of wave parameters). As shown in figure 3, the numerical studies by Xiao *et al.* (2013) indicate an initial overshoot of the kurtosis followed by a decay towards quasi-Gaussian conditions.

In particular, figure 3(*a*) shows that for a narrow directional spreading ($\sigma_\theta \sim 0.04$) the present theoretical NB model (thick line) explains the peak kurtosis and the initial transient behaviour of BMNLS simulations (thin dashed line) as NB is consistent with the dynamics of the 2-D NLS equation. BMNLS and NB yield faster initial growth and overestimate both HOS (thin solid line) and experiments (triangle symbols). However, soon after the transient stage, the spectrum has already broadened in frequency and spread angularly, approaching a quasi-equilibrium state. At this stage, the NB approximation provides just a qualitative trend of the large-time behaviour since it does not account for spectral changes. In particular, NB shows a slower decaying trend to zero than BMNLS. This indicates that numerical models capture the directional energy spreading and quasi-resonant interactions attenuate much faster than NB after the transient peak.

For a broad directional spreading ($\sigma_\theta \sim 0.07$) figure 3(*b*) shows that NB overestimates the maximum kurtosis and qualitatively explains the initial transient overshoot of BMNLS simulations, which are now beyond their range of validity as the spectrum

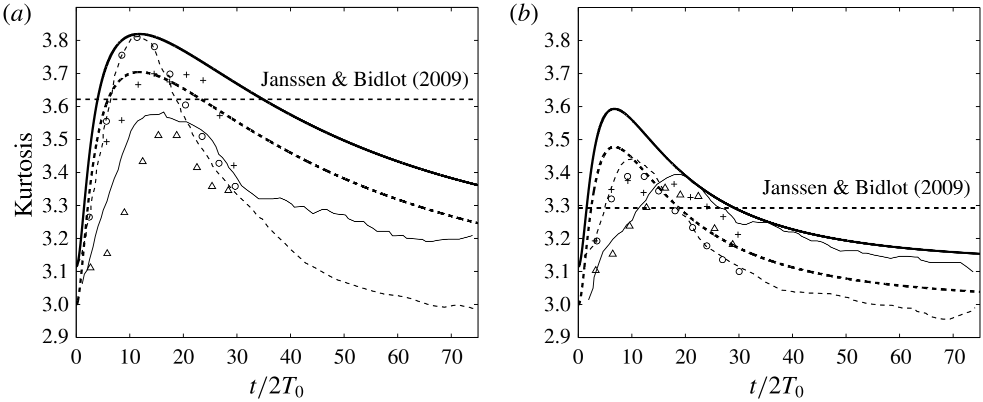

FIGURE 3. Kurtosis $\mu_4 = \langle\eta^4\rangle/\langle\eta^2\rangle^2 = 3(C_4+1)$ as a function of time $t/2T_0$ for JONSWAP directional wave fields initially homogeneous and Gaussian (BFI = 0.78, μ = 0.08, $\nu = 0.15$): theoretical narrowband predictions compared to simulations and experiments ($\triangle$) from Onorato *et al.* (2009) (data digitized from figure 10*a*,*b* in Xiao *et al.* 2013). (*a*) Narrow directional spreading with $\sigma_\theta = 0.04$, $R = 0.03$ (see (2.9)) and (*b*) broad directional spreading with $\sigma_\theta = 0.07$, $R = 0.1$. Narrowband theory: dynamic kurtosis $\mu_4^d = 3(C_4^d + 1)$ from (2.10) (thick dashed line) and total kurtosis $\mu_4 = \mu_4^d + \mu_4^b$ (thick solid line), with $\mu_4^b = 3(C_4^b + 1)$ from (1.3). Dashed horizontal lines denote Janssen & Bidlot (2009) dynamic kurtosis maximum from (4.6) with $b = 1$. Simulation results from Xiao *et al.* (2013): HOS (thin solid line), BMNLS (thin dashed line). The numerical results from Toffoli *et al.* (2010) are also shown: BMNLS ($\bigcirc$) and HOS (+).

is already too broad initially. Instead, HOS simulations are in agreement with experiments and yield a smaller value of the maximum kurtosis and a slower transient than BMNLS. This suggests that higher order-nonlinearities and broader spectral bandwidth effects should be accounted for to obtain more accurate theoretical models for kurtosis evolution. Indeed, for the compact form of the 1-D Zakharov equation (cDZ, Dyachenko & Zakharov 2011), Fedele (2014) showed that, correct to $O(\nu^2)$ in spectral bandwidth, the associated dynamic kurtosis maximum

$$C^d_{4,cDZ} = C^d_{4,NLS}\left(1 - \frac{4\sqrt{3}+\pi}{8\pi}\nu^2\right) \approx C^d_{4,NLS}(1 - 0.40\nu^2) \tag{5.1}$$

is smaller than the NLS counterpart $C^d_{4,NLS}$ in (1.4), especially as the spectrum widens. The present study can be extended to derive an analytical solution of the kurtosis evolution from initial Gaussian and homogeneous wave conditions in accord with the 2-D Zakharov equation (Dyachenko & Zakharov 2011; Gramstad 2014).

Finally, we note that in both the above-mentioned cases the NB model qualitatively describes the initial transient and kurtosis peak. For time scales $t \gg t_c$, NB indicates the correct asymptotic behaviour of the total kurtosis of surface elevations as dominated by nonlinear bound harmonics (see also Annenkov & Shrira 2013 and Annenkov & Shrira 2014).

6. Concluding remarks

Our refinement of Janssen's (2003) theory implies that in typical multidirectional or short-crested oceanic fields third-order quasi-resonant interactions do not appear to play a significant role in the wave growth. In particular, we have shown that the large excess dynamic kurtosis transient observed during the initial stage of wave evolution is a result of the unrealistic assumption that the initial wave field is homogeneous Gaussian. A random wave field forgets its initial conditions and adjusts to a non-Gaussian state dominated by bound nonlinearities in agreement with experiments (Onorato *et al.* 2009; Waseda *et al.* 2009) and simulations (Annenkov & Shrira 2013, 2014). In this regime, statistical predictions of rogue waves can be based on the Tayfun (1980) and Janssen (2009) models to account for both second-order skewness and third-order bound kurtosis nonlinearities (Fedele 2015).

Acknowledgements

F.F. is grateful to P. A. E. M. Janssen for suggesting the topic of this work and for discussions on nonlinear water waves. F.F. also thanks M. L. Banner, V. Shrira and M. A. Tayfun for discussions on nonlinear wave statistics and random wave fields.

Appendix A

Consider the generic sixfold integral

$$J_0(\tau; P, Q) = 2\,\mathrm{Re}\int \frac{1-\exp(\mathrm{i}\Delta\tau)}{\Delta}\widetilde{E}_1\widetilde{E}_2\widetilde{E}_3\,\mathrm{d}v_{1,2,3}\,\mathrm{d}\phi_{1,2,3}, \tag{A 1}$$

where P and Q are complex coefficients,

$$\Delta = P\Delta_v - Q\Delta_\phi \tag{A 2}$$

and

$$\widetilde{E}_j(v_j, \phi_j) = \frac{\exp\left(-\dfrac{v_j^2+\phi_j^2}{2}\right)}{2\pi}. \tag{A 3}$$

Then, the integral (A 1) can be written as

$$\begin{aligned} J_0(\tau; P, Q) &= \mathrm{Re}\int \frac{1-\exp(\mathrm{i}P\Delta_v\tau - \mathrm{i}Q\Delta_\phi\tau)}{P\Delta_v - \mathrm{i}Q\Delta_\phi}\frac{\exp\left(-\dfrac{v_1^2+v_2^2+v_3^2}{2}\right)}{(2\pi)^{3/2}} \\ &\quad\times \frac{\exp\left(-\dfrac{\phi_1^2+\phi_2^2+\phi_3^2}{2}\right)}{(2\pi)^{3/2}}\,\mathrm{d}v_{1,2,3}\,\mathrm{d}\phi_{1,2,3}. \end{aligned} \tag{A 4}$$

Clearly, v_j and ϕ_j are coupled via the denominator $P\Delta_v - \mathrm{i}Q\Delta_\phi$. However, they become uncoupled if we take the time derivative

$$\begin{aligned} \frac{\mathrm{d}J_0}{\mathrm{d}\tau} &= \mathrm{Im}\int \exp(\mathrm{i}P\Delta_v\tau - \mathrm{i}Q\Delta\tau)\frac{\exp\left(-\dfrac{v_1^2+v_2^2+v_3^2}{2}\right)}{(2\pi)^{3/2}} \\ &\quad\times \frac{\exp\left(-\dfrac{\phi_1^2+\phi_2^2+\phi_3^2}{2}\right)}{(2\pi)^{3/2}}\,\mathrm{d}v_{1,2,3}\,\mathrm{d}\phi_{1,2,3}. \end{aligned} \tag{A 5}$$

Indeed,

$$\frac{\mathrm{d}J_0}{\mathrm{d}\tau} = 2\,\mathrm{Im}[I_0(\tau; P)I_0(\tau; -Q)], \tag{A 6}$$

where

$$I_0(\tau; P) = \int \exp(\mathrm{i}P\Delta_z\tau)\frac{\exp\left(-\dfrac{z_1^2+z_2^2+z_3^2}{2}\right)}{(2\pi)^{3/2}}\,\mathrm{d}z_{1,2,3}. \tag{A 7}$$

Drawing on Fedele *et al.* (2010) Gaussian integration yields

$$I_0(\tau; P) = \frac{1}{\sqrt{1-2\mathrm{i}P\tau+3P^2\tau^2}} \tag{A 8}$$

and from (A 6)

$$\frac{\mathrm{d}J_0(\tau; P, Q)}{\mathrm{d}\tau} = 2\,\mathrm{Im}\left(\frac{1}{\sqrt{1-2\mathrm{i}P\tau+3P^2\tau^2}\sqrt{1+2\mathrm{i}Q\tau+3Q^2\tau^2}}\right). \tag{A 9}$$

Appendix B

Recently, Toffoli *et al.* (2010) and Xiao *et al.* (2013) have compared BMNLS and HOS simulations of JONSWAP directional wave fields to the experimental results in Onorato *et al.* (2009). Their Benjamin–Feir index is a factor $\sqrt{2}$ larger than the one used in this work (see (1.5)), that is

$$\mathrm{BFI}' = \frac{2k_0\sigma}{\nu} = \frac{2\mu}{\nu} = \sqrt{2}\mathrm{BFI}. \tag{B 1}$$

Further, their wave steepness $\mu' = 2\mu$ where $\mu = k_0\sigma$ is used in this work (see also table 1 in Toffoli *et al.* 2010). In the numerical results reported in figure 10(*a*,*b*) of Xiao *et al.* (2013), $\mathrm{BFI}' = 1.1$ and $\mu' = 0.16$. Thus, $\mathrm{BFI} = 0.78$, $\mu = 0.08$ and the spectral bandwidth follows as $\nu = \sqrt{2}\mu/\mathrm{BFI} = 0.15$.

The directional distribution $D(\theta)$ adopted by Xiao *et al.* (2013) is given by

$$D(\theta) = \frac{2}{\Theta}\cos^2\left(\frac{\pi\theta}{\Theta}\right), \quad |\theta| \leqslant \frac{\Theta}{2} \tag{B 2a,b}$$

and the associated directional spreading follows as

$$\sigma_\theta = \sqrt{\frac{\displaystyle\int_{-\Theta/2}^{\Theta/2} D(\theta)\theta^2\,\mathrm{d}\theta}{\displaystyle\int_{-\Theta/2}^{\Theta/2} D(\theta)\,\mathrm{d}\theta}} = \Theta\sqrt{\frac{\pi^2-6}{12\pi^2}}. \tag{B 3}$$

The numerical results shown in figure 10(*a*) of Xiao *et al.* (2013) are for $\Theta = 12(\pi/180)$ rad (narrow directional spreading); using (B 3) yields $\sigma_\theta = 0.04$ and $R = 0.03$ from (2.9). For the case of broad directional spreading shown in their figure 10(*b*) $\Theta = 21(\pi/180)$ rad and $\sigma_\theta = 0.07$, $R = 0.1$.

REFERENCES

ANNENKOV, S. Y. & SHRIRA, V. I. 2013 Large-time evolution of statistical moments of wind–wave fields. *J. Fluid Mech.* **726**, 517–546.

ANNENKOV, S. Y. & SHRIRA, V. I. 2014 Evaluation of skewness and kurtosis of wind waves parameterized by jonswap spectra. *J. Phys. Oceanogr.* **44** (6), 1582–1594.

CHABCHOUB, A., HOFFMANN, N. P. & AKHMEDIEV, N. 2011 Rogue wave observation in a water wave tank. *Phys. Rev. Lett.* **106**, 204502.

CHABCHOUB, A., HOFFMANN, N., ONORATO, M. & AKHMEDIEV, N. 2012 Super rogue waves: Observation of a higher-order breather in water waves. *Phys. Rev.* X **2**, 011015.

DOMMERMUTH, D. G. & YUE, D. K. P. 1987 A high-order spectral method for the study of nonlinear gravity waves. *J. Fluid Mech.* **184**, 267–288.

DYACHENKO, A. I. & ZAKHAROV, V. E. 2011 Compact equation for gravity waves on deep water. *J. Expl Theor. Phys. Lett.* **93** (12), 701–705.

DYSTHE, K. B. 1979 Note on a modification to the nonlinear Schrödinger equation for application to deep water. *Proc. R. Soc. Lond.* A **369**, 105–114.

FEDELE, F. 2008 Rogue waves in oceanic turbulence. *Physica* D **237**, 2127–2131.

FEDELE, F. 2014 On certain properties of the compact Zakharov equation. *J. Fluid Mech.* **748**, 692–711.

FEDELE, F. 2015 On oceanc rogue waves. Preprint, arXiv:1501.03370.

FEDELE, F., CHERNEVA, Z., TAYFUN, M. A. & SOARES, C. G. 2010 Nonlinear schrodinger invariants and wave statistics. *Phys. Fluids* **22** (3), 036601.

FEDELE, F. & TAYFUN, M. A. 2009 On nonlinear wave groups and crest statistics. *J. Fluid Mech.* **620**, 221–239.

GRAMSTAD, O. 2014 The zakharov equation with separate mean flow and mean surface. *J. Fluid Mech.* **740**, 254–277.

JANSSEN, P. A. E. M. 2003 Nonlinear four-wave interactions and freak waves. *J. Phys. Oceanogr.* **33** (4), 863–884.

JANSSEN, P. 2009 On some consequences of the canonical transformation in the Hamiltonian theory of water waves. *J. Fluid Mech.* **637**, 1–44.

JANSSEN, P. A. E. M. 2014*a* Notes on kurtosis evolution for 2d wave propagation. Memorandum Research Department 60.9/PJ/0387. ECMWF.

JANSSEN, P. A. E. M. 2014*b* On a random time series analysis valid for arbitrary spectral shape. *J. Fluid Mech.* **759**, 236–256.

JANSSEN, P. A. E. M. & BIDLOT, J. R. 2009 On the extension of the freak wave warning system and its verification. *Tech. Memo* 588. ECMWF.

KRASITSKII, V. P. 1994 On reduced equations in the Hamiltonian theory of weakly nonlinear surface waves. *J. Fluid Mech.* **272**, 1–20.

MORI, N. & JANSSEN, P. A. E. M. 2006 On kurtosis and occurrence probability of freak waves. *J. Phys. Oceanogr.* **36** (7), 1471–1483.

ONORATO, M., CAVALERI, L., FOUQUES, S., GRAMSTAD, O., JANSSEN, P. A. E. M., MONBALIU, J., OSBORNE, A. R., PAKOZDI, C., SERIO, M., STANSBERG, C. T., TOFFOLI, A. & TRULSEN, K. 2009 Statistical properties of mechanically generated surface gravity waves: a laboratory experiment in a three-dimensional wave basin. *J. Fluid Mech.* **627**, 235–257.

SHEMER, L. & ALPEROVICH, S. 2013 Peregrine breather revisited. *Phys. Fluids* **25**, 051701.

SHEMER, L. & LIBERZON, D. 2014 Lagrangian kinematics of steep waves up to the inception of a spilling breaker. *Phys. Fluids* **26** (1), 016601.

SHEMER, L. & SERGEEVA, A. 2009 An experimental study of spatial evolution of statistical parameters in a unidirectional narrow-banded random wavefield. *J. Geophys. Res.* **114**, C01015.

SHEMER, L., SERGEEVA, A. & LIBERZON, D. 2010*a* Effect of the initial spectrum on the spatial evolution of statistics of unidirectional nonlinear random waves. *J. Geophys. Res.* **115**, C12039.

SHEMER, L., SERGEEVA, A. & SLUNYAEV, A. 2010*b* Applicability of envelope model equations for simulation of narrow-spectrum unidirectional random wave field evolution: experimental validation. *Phys. Fluids* **22** (1), 016601.

TAYFUN, M. A. 1980 Narrow-band nonlinear sea waves. *J. Geophys. Res.* **85** (C3), 1548–1552.

TAYFUN, M. A. & FEDELE, F. 2007 Wave-height distributions and nonlinear effects. *Ocean Engng* **34** (11–12), 1631–1649.

TAYFUN, M. A. & LO, J. 1990 Nonlinear effects on wave envelope and phase. *J. Waterways Port Coast. Ocean Engng* **116**, 79–100.

TOFFOLI, A., GRAMSTAD, O., TRULSEN, K., MONBALIU, J., BITNER-GREGERSEN, E. & ONORATO, M. 2010 Evolution of weakly nonlinear random directional waves: laboratory experiments and numerical simulations. *J. Fluid Mech.* **664**, 313–336.

WASEDA, T., KINOSHITA, T. & TAMURA, H. 2009 Evolution of a random directional wave and freak wave occurrence. *J. Phys. Oceanogr.* **39** (3), 621–639.

XIAO, W., LIU, Y., WU, G. & YUE, D. K. P. 2013 Rogue wave occurrence and dynamics by direct simulations of nonlinear wave-field evolution. *J. Fluid Mech.* **720**, 357–392.

ZAKHAROV, V. E. 1968 Stability of periodic waves of finite amplitude on the surface of a deep fluid. *J. Appl. Mech. Tech. Phys.* **9**, 190–194.

ZAKHAROV, V. E. 1999 Statistical theory of gravity and capillary waves on the surface of a finite-depth fluid. *Eur. J. Mech. (*B*/Fluids)* **18** (3), 327–344.